Electron–longitudinal-optical-phonon coupling and intersubband scattering in modulation-doped quantum wells under high-electric-field transport conditions

C. Guillemot, F. Clérot, and A. Regreny
Centre National d'Etudes Télécommunications, 22301 Lannion CEDEX, France
(Received 12 February 1992; revised manuscript received 27 May 1992)

The electron–longitudinal-optical-phonon coupling in $GaAs/Ga_xAl_{1-x}As$ modulation-doped quantum wells is studied under the conditions of steady-state high-field transport from theoretical and experimental points of view. The calculations are based on the Lei-Ting approach of high-field transport in a two-subband system. A common hot-electron temperature is assumed for both subbands but the Fermi levels are allowed to split off because of the weakness of the intersubband Coulomb interaction against the impurity and LO-phonon intersubband scatterings. The agreement with experiments requires a phonon lifetime of about 5 ps and a nonequilibrium hot-phonon population drifting with the electron gas. Moreover, we show that the temperature versus power-loss diagrams do not fully characterize the electron–LO-phonon coupling since this coupling increases with the drift velocity through the Doppler shift of the LO-phonon frequency. Finally, for a vanishing electric field, the low-temperature mobility is shown theoretically to be mainly reduced at the onset of the second subband by intrasubband scattering. It is argued that the high-mobility electrons lying at the Fermi level of the ground subband are efficiently scattered within their subband by the low-mobility carriers of the upper subband through the electron-electron Coulomb interaction.

I. INTRODUCTION

In recent years, considerable interest has been focused on the development of a full understanding of the hot-electron energy-loss rate in quasi-two-dimensional heterosystems, under conditions of steady-state high-field transport or optical pumping.[1–6] The energy loss rate of a quasi-two-dimensional electron gas (2DEG) in modulation-doped multiple quantum wells, measured in steady-state transport experiments,[1,7,8] is about one order of magnitude smaller than the theoretically predicted value for high-electron-density samples. The proposed explanation for this anomalously low electron-energy-loss rate is based on the assumption of a nonequilibrium population of longitudinal-optical (LO) phonons, in excess of what is to be expected at the lattice temperature. During the cooling of the electron gas by the emission of LO phonons, there is a finite probability that an emitted LO phonon will be reabsorbed by the hot-electron gas before decaying into acoustic phonons via anharmonic processes if the LO-phonon-population lifetime is nonzero, as is suggested by time-resolved experiments.[9–11]

The LO-phonon lifetime in a single lattice mode or dephasing time may be shorter than the relaxation time of the population of all the modes with a common wave-vector module, if the LO-phonon momentum is efficiently relaxed within the LO-phonon modes by intrabranch scattering events; these could originate from alloy fluctuations in the barrier or interface roughness. In such a case, hot LO phonons are nondrifting and although the energy-relaxation rate of the electron gas is slowed down by the hot-phonon reabsorption, the electron-gas momentum-relaxation rate is enhanced, reducing the drift velocity at high electric fields.[12] Conversely, if the LO-phonon population lifetime is also the momentum relaxation time, there will be little reduction in the electron-gas momentum-relaxation rate since the momentum will be reabsorbed together with the energy of the phonon mode.

Besides, the experimental electron-energy-loss rate deduced from transport experiments also depends on the drift velocity. Because the electron gas is drifting with reference to the lattice, the effective LO-phonon frequency is Doppler shifted from ω_{LO} to $\omega_{LO}-\mathbf{v}_d\cdot\mathbf{q}$, where $\mathbf{v}_d$ is the drift velocity and $\mathbf{q}$ the wave vector of the phonon mode. The difference between these two frequencies amounts to the electric-field energy, which is transferred to the LO-phonon bath without being degraded into heat. Therefore, the lower the drift velocity, the hotter the electron gas for a given electric-field power input.

The drift velocity may be greatly reduced if intersubband scattering takes place as should be the case for some large quantum wells that have been experimentally investigated.[1,8] On the other hand, the increase of the density of states associated with the occurrence of a second subband should increase the energy-loss rate of the electron gas, owing to the new allowed electronic transitions involving a LO-phonon emission. However, in such circumstances, Coulomb interactions must be carefully handled. First, many-body interactions within the electron gas shift and broaden the single-particle states and, consequently, the energy spreading between the subbands is determined not only by the quantum-well width but also by the electron-gas density and its temperature. Moreover, Coulomb interactions are known to be efficient in giving a unique temperature within both subbands but they are likely to fail to give a common Fermi level because the exchange of particles between the subbands

through Coulomb interactions involves form factors that are quite small. Then, the electronic population and the Fermi level within each subband may be determined by particle exchange due to phonon- or impurity-intersubband scattering rather than by Coulomb interactions. Therefore, the emission of LO phonons due to electronic transitions from the upper to the ground subband lowers the Fermi level in the upper subband. As a consequence, in order to keep the same average energy per electron, the temperature of the electron gas should be raised, compared to what it would be for an electron gas in a fully equilibrium state.

The purpose of the present paper is to investigate how the energy and momentum loss rates of a 2DEG under a high electric field in a modulation-doped GaAs/$Ga_xAl_{1-x}As$ quantum well, are modified by the LO-phonon lifetime, the drift velocity, and intersubband scattering. The investigations reported here are based on the balance description of high-field transport of Lei and Ting.[13] In the second section, we shall rederive the main results of the balance equation theory following Lei and Ting's original paper, but extending it in order to allow explicitly for different Fermi levels in each subband. Many-body properties such as screening or renormalization are handled within the random-phase approximation (RPA) in a two-subband system at finite temperature. In the third section, we shall derive the zero-temperature impurity-limited low-field resistivity within a two subbands system. We shall discuss the difference between our result (at the onset of the second subband, the main mechanism reducing the mobility is the intrasubband scattering rate rather than the intersubband scattering rate) and the conductivity derived from coupled Boltzmann equations.[14] In the fourth section, we present experimental and theoretical results and discuss the dependence of the drift velocity and of the electron-energy-loss rate on parameters such as the LO-phonon lifetime and the low-field, low-temperature mobility.

II. BALANCE EQUATIONS

We consider a quantum well of width L and barrier height V, and denote by N the two-dimensional electron-gas density. The growth axis is in the z direction. In the following, a uniform background static dielectric constant κ is assumed and the in-plane electronic properties are described through an effective mass m. A constant uniform electric field $\mathbf{E}=E_x\mathbf{x}$ is applied in the plane of the quantum well. Electrons are scattered by randomly located impurities ($H_{e\text{-imp}}$) and are coupled with phonons ($H_{e\text{-ph}}$).

Following Lei and Ting, we can separate the electronic degrees of freedom into a center-of-mass part ($H_{\text{c.m.}}$) and a relative 2DEG part (H_e) by introducing

$$\mathbf{P}=\sum_{i=1}^{N}\mathbf{p}_i,\quad \mathbf{R}=(1/N)\sum_{i=1}^{N}\mathbf{r}_i\ ,$$

$$\mathbf{r}'_i=\mathbf{r}_i-\mathbf{R},\quad \mathbf{p}'_i=\mathbf{p}_i-\mathbf{P}/N\ ,$$

$$\text{with } [r'_{i\alpha},p'_{j\beta}]=i\hbar\delta_{\alpha,\beta}[\delta_{i,j}-1/N],\quad [R_\alpha,P_\beta]=i\hbar\delta_{\alpha,\beta}\ .$$

Here $\mathbf{r}_i$ and $\mathbf{p}_i$ are the position and the momentum of the ith electron, whereas $\mathbf{r}'_i$ and $\mathbf{p}'_i$ are the corresponding relative-coordinate variables. $\mathbf{P}$ and $\mathbf{R}$ are the center-of-mass momentum and position operators. The commutation relations between $\mathbf{r}'_i$ and $\mathbf{p}'_j$ are not exactly canonical because the relative electrons are not completely independent with $2N$ degrees of freedom but are subject to constraints:

$$\sum_{j=1}^{N}\mathbf{p}'_j=0,\quad \sum_{i=1}^{N}\mathbf{r}'_i=0\ .$$

These constraints can be ignored and the relative coordinate variables can be considered as canonical ones, provided only the lowest-order terms in the scattering interactions (impurities and phonons) are retained in the description of the relative electron gas state and that the fluctuations of the center-of-mass position are ignored: because of its enormous mass Nm, the center-of-mass motion is nearly classical.[15]

The total Hamiltonian of the system can thus be written as

$$H=H_{\text{c.m.}}+H_e+H_{\text{ph}}+H_{e\text{-imp}}+H_{e\text{-ph}}+H_{\text{ph-ph}}\ ,$$

where

$$H_{\text{c.m.}}=\mathbf{P}^2/(2Nm)-Ne\mathbf{E}\cdot\mathbf{R}\ ,$$

$$H_e=H_{\text{kin}}+H_{\text{Cou}}=\sum_{\mathbf{k},s,\sigma}\epsilon_{\mathbf{k}}c^{\dagger}_{\mathbf{k},s,\sigma}c_{\mathbf{k},s,\sigma}$$
$$+\tfrac{1}{2}\sum_{\substack{\mathbf{q}\neq 0\\ \sigma_1,\sigma_2,\sigma_3,\sigma_4}}F^{\sigma_3,\sigma_4}_{\sigma_1,\sigma_2}(\mathbf{q})e^2/(2A\epsilon_0\kappa q)\left[\sum_{\mathbf{k},s,\mathbf{k}',s'}c^{\dagger}_{\mathbf{k}+\mathbf{q},s,\sigma_2}c^{\dagger}_{\mathbf{k}'-\mathbf{q},s',\sigma_4}c_{\mathbf{k}',s',\sigma_3}c_{\mathbf{k},s,\sigma_1}\right]\ ,$$

$$H_{\text{ph}}=H^{\text{ac}}_{\text{ph}}+H^{\text{opt}}_{\text{ph}}\ ,$$

$$H^{\text{ac}}_{\text{ph}}=\sum_{Q,\lambda}\hbar\omega_{Q,\lambda}(b^{\dagger}_{Q,\lambda}b_{Q,\lambda}+\tfrac{1}{2})\ ,$$

$$H^{\text{opt}}_{\text{ph}}=\sum_{\mathbf{q},\lambda}\hbar\omega_{\text{LO}}(b^{\dagger}_{\mathbf{q},\lambda}b_{\mathbf{q},\lambda}+\tfrac{1}{2})\ ,$$

$$H_{e\text{-imp}}=\sum_{i,\sigma,\sigma'}[G^{\sigma'}_{\sigma}(\mathbf{z}_i,\mathbf{q})e^2/(2A\epsilon_0\kappa q)]e^{i\mathbf{q}\cdot(\mathbf{R}-\mathbf{R}_i)}\rho^{\sigma'}_{\sigma}(\mathbf{q})\ ,$$

$$H_{e\text{-ph}}=\sum_{q,\lambda,\sigma,\sigma'} M_{\text{opt}}(\mathbf{q},\lambda)I_{\sigma}^{\sigma'}(\lambda,\mathbf{q})(b_{\mathbf{q},\lambda}+b^{\dagger}_{-\mathbf{q},\lambda})e^{i\mathbf{q}\cdot\mathbf{R}}\rho_{\sigma}^{\sigma'}(\mathbf{q}) + \sum_{\mathbf{q},q_z,\lambda,\sigma,\sigma'} M_{\text{ac}}(\mathbf{Q},\lambda)I_{\sigma}^{\sigma'}(q_z)(b_{\mathbf{Q},\lambda}+b^{\dagger}_{-\mathbf{Q},\lambda})e^{i\mathbf{q}\cdot\mathbf{R}}\rho_{\sigma}^{\sigma'}(\mathbf{q}) ,$$

where σ is a subband index and the other symbols have their usual meaning.[8,13]

We assume the acoustic phonons to be the GaAs acoustic modes because the GaAs and $Ga_xAl_{1-x}As$ bulk-material velocities of sound are quite similar, and intrasubband scattering only will be taken into account for the electron-acoustic phonon coupling.

The quantized LO-phonon modes (q,λ) are derived through a model for long-wavelength longitudinal-optical phonons, which is based on the framework of the Born-Huang model generalized to include the isotropic dispersion effects in the Brillouin-zone center.[16] The essential requirement of mutual orthogonality of the different eigenmodes is fulfilled, and the Maxwell equations are verified. For double heterostructures, there are a finite number of confined quantized modes exhibiting, in part, a Coulomb or interface-mode behavior. The phonon-phonon interaction $H_{\text{ph-ph}}$ will be heuristically modeled by a unique LO-phonon relaxation time τ_{ph} in the kinetic equation for the LO-phonon occupation numbers $N_{\mathbf{q},\lambda}=b^{\dagger}_{\mathbf{q},\lambda}b_{\mathbf{q},\lambda}$. Therefore, we assume that the dephasing time is equal to the population relaxation time ("drifting hot phonons"). Comparing theoretical and experimental results, we shall show later that this assumption is reasonable.

For the electron-LO phonon interaction, we have retained only the four higher modes (two of them are even and two are odd) since they give more than 95% of the total electron–LO-phonon scattering rate. For the quantum well widths that will be considered here, the quantization of the LO-phonon modes is not essential and results would not change if bulk LO phonons were used.

The electron-electron Coulomb interaction arises through form factors, such as

$$F_{\sigma_1,\sigma_2}^{\sigma_3,\sigma_4}(\mathbf{q})=\int\int d\mathbf{z}\,d\mathbf{z}'\zeta^{*}_{\sigma_2}(\mathbf{z})\zeta^{*}_{\sigma_4}(\mathbf{z}')\zeta_{\sigma_3}(\mathbf{z}')\zeta_{\sigma_1}(\mathbf{z}) \times\exp(-\mathbf{q}\cdot|\mathbf{z}-\mathbf{z}'|) ,$$

describing the collision between an electron in subband σ_1 and an electron in subband σ_3, which are scattered, respectively, into subband σ_2 and subband σ_4. In symmetric quantum wells, only four form factors are nonzero in a two-subband model (the ground subband is labeled 0 and the upper subband is labeled 1): $F_{0,0}^{0,0}$ and $F_{1,1}^{1,1}$ are involved in pure intrasubband Coulomb scattering. These collisions tend to establish a temperature within each subband. $F_{0,0}^{1,1}$ describes the collisions between electrons belonging to different subbands but which are scattered within the same subband. This kind of collision tends to give a unique temperature for both subbands. $F_{0,1}^{0,1}$, $F_{0,1}^{1,0}$, $F_{1,0}^{0,1}$, and $F_{1,0}^{1,0}$ involve exchange of particles between the two subbands with the conservation of the number of electrons within each subband $(F_{0,1}^{1,0},F_{1,0}^{0,1})$ or with the transfer of two electrons from one subband to the other $(F_{0,1}^{0,1},F_{1,0}^{1,0})$. All these form factors have the same value and are small as compared to $F_{0,0}^{0,0}$, $F_{1,1}^{1,1}$, and $F_{0,0}^{1,1}$, because they vanish for $\mathbf{q}=\mathbf{0}$. Hence, the Coulomb interaction H_{Cou} can be separated in two parts: H_{Cou}^{T} (made up of terms containing $F_{0,0}^{0,0}$, $F_{1,1}^{1,1}$, and $F_{0,0}^{1,1}$, which tends to give a unique electronic temperature in both subbands and H_{Cou}^{F} (made up of the remaining smaller terms), which tends to establish a unique Fermi level within both subbands.

Ignoring the fluctuations of the center-of-mass coordinates, we write $\mathbf{R}=\mathbf{v}_d t$. The relative electron gas and the phonon bath are fully described by $H-H_{\text{c.m.}}$, independently of the center-of-mass Hamiltonian and of the electric field. To determine the steady state of the relative electron gas and of the phonon bath through the Liouville equation on the density matrix Ξ,

$$\frac{i\hbar d\Xi}{dt}=[H_{\text{kin}}+H_{\text{Cou}}^{T}+H_{\text{ph}}+H_I+H_{\text{Cou}},{}^{F}\Xi]$$

$$\text{with } H_I=H_{e\text{-imp}}+H_{e\text{-ph}}+H_{\text{ph-ph}} ,$$

we need to start with an initial state Ξ_0 as close as possible to the final steady state. Since H_I can be handled perturbatively against $H_0=H_{\text{kin}}+H_{\text{Cou}}^{T}+H_{\text{ph}}$ and assuming that the Coulomb terms H_{Cou}^{F} can be neglected as compared to H_I, we imagine turning off all the electron-impurity, electron-phonon, and phonon-phonon interactions and the electric field.[13] Then, the center of mass and the relative electron system are decoupled from each other. The center of mass is moving freely with the drift velocity of the final steady state, whereas each subband of the relative electron system approaches a thermal equilibrium with a unique temperature T_e because of the Coulomb interactions H_{Cou}^{T} but with its own Fermi level: since the exchange of electrons between the subbands was governed by the intersubband parts of $H_{e\text{-imp}}$ and $H_{e\text{-ph}}$, no more exchange of particles is allowed between the subbands. The optical and acoustical phonons are also decoupled; as the sample is in contact with a heat reservoir at temperature T (helium bath), acoustic phonons remain in a quasiequilibrium state at temperature T ("lattice temperature"). The nonequilibrium optical-phonon distribution is allowed through a temperature $T_{\lambda,\mathbf{q}}$ for each mode. Therefore, the initial density matrix is chosen as

$$\Xi_0=\{\exp[-\beta_e(H_{\rm kin}+H^T_{\rm Cou}-\mu_0 N_0-\mu_1 N_1)]/Z_e\}\left[\prod_\lambda \exp(-\beta H^{\rm ac}_\lambda)/Z_\lambda\right]\left[\prod_{\lambda,\mathbf{q}} \exp(-\beta_{\lambda,\mathbf{q}}H^{\rm opt}_\lambda,\mathbf{q})\Big/Z_{\lambda,\mathbf{q}}\right]$$

with

$$\beta_e=1/kT_e,\ \beta=1/kT,\ \beta_{\lambda,q}=1/kT_{\lambda,q},\ N_0=\prod_{\mathbf{k},s} c^\dagger_{\mathbf{k},s,0}c_{\mathbf{k},s,0},\ N_1=\prod_{\mathbf{k},s} c^\dagger_{\mathbf{k},s,1}c_{\mathbf{k},s,1}\ \ (N=N_0+N_1)\ ,$$

where μ_0 and is the Fermi level in the bottom subband, μ_1 is the Fermi level in the top subband, and k is the Boltmann constant.

We then solve the Liouville equation for the density matrix $\Xi(t)$ to first order in H_I, with the initial condition Ξ_0. The final steady state is characterized by

$$\langle \dot{\mathbf{P}} \rangle = 0 \quad \text{(constant momentum of the center of mass)}\ , \tag{1}$$

$$\langle \dot{H}_e \rangle = 0 \quad \text{(constant energy of the relative electrons)}\ , \tag{2}$$

$$\langle \dot{N}_0 \rangle = -\langle \dot{N}_1 \rangle = 0 \quad \text{(constant populations in each subband)}\ , \tag{3}$$

$$\langle \dot{N}_{\lambda,\mathbf{q}} \rangle = (1/i\hbar)[N_{\lambda,\mathbf{q}}, H_{e\text{-ph}}] - (N_{\lambda,\mathbf{q}}-N_{eq})/\tau_{\rm ph} = 0 \quad \text{(constant LO-phonon population in each mode)}\ . \tag{4}$$

The full expression of Eqs. (1)–(4) is given in Appendix A.

In the above equations, the many-body properties of the two subband electron gas (renormalization energies and polarizability) are taken into account in the finite-temperature dynamical RPA formalism.[17] Those calculations are self-consistent in the sense that the broadening of the electronic states is taken into account in the calculation of the electron self-energy.[18] In agreement with Ref. 19, we find that intersubband exchange cannot be neglected, since it renormalizes the upper subband by about half the renormalization energy of the lower subband, which is mainly due to intrasubband processes.

The numerical solution of the nonlinear system (1)–(4) enables us to determine the unknown parameters $\mathbf{v}_d, T_e, T_{\lambda,q}, \Delta\mu=\mu_1-\mu_0$.

III. LOW-FIELD MOBILITY

First, we discuss the solution of the balance equations (1)–(4), in the zero-field limit. For a zero electric field, $T_e=T$ and $\Delta\mu=0$ are obvious solutions. Developing the balance equations to first order in the electric field, it is easy to show that both derivatives dT_e/dE and $d\Delta\mu/dE$ are zero at vanishing electric field: the subband Fermi levels are equal when the electric field is handled to first order. It also follows that the LO-phonon population is the equilibrium one at temperature T.

The total resistivity is the sum of the different scattering rates, due to impurities or phonons, intrasubband or intersubband. To go further, we will consider only impurity-limited Ohmic resistivity at zero temperature. It can be split into two contributions, an intraband and an interband resistivity:

$$R_{2\,\rm DEG}=(1/Ne)(1/\mu)=(1/Ne)(m/e)(R_{\rm intra}+R_{\rm inter})\ ,$$

where μ is the mobility and R refers to a scattering rate. The full expressions of the scattering rates $R_{\rm intra}$ and $R_{\rm inter}$ are given in Appendix B.

We plot in Fig. 1, the intrasubband and intersubband scattering rates for a 25-nm-large quantum well. Electrons are scattering on 7.5×10^{11} cm^{-2} remote impurities located 25 nm away from the quantum-well interfaces. Two main features should be emphasized: first the mobility drop only occurs in a limited 2DEG density range, and second the main scattering mechanism reducing the mobility at the onset of the upper subband is the in-

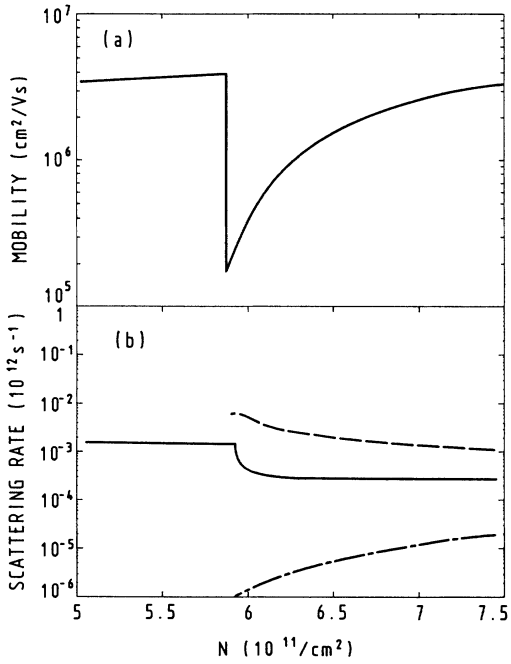

FIG. 1. (a) Zero-temperature mobility vs the 2DEG density. (b) Scattering rates vs the 2DEG density: intersubband scattering rate (dashed-dotted curve); intrasubband scattering rate $(N_0/N)R_0$ within the ground subband (full curve), and the intrasubband scattering rate $(N_1/N)R_1$ within the upper subband (dashed curve).

trasubband scattering rate R_{intra}. This is at variance with the results derived from coupled Boltzmann equations,[14] where the intersubband scattering was claimed to reduce the mobility in a wide 2DEG density range above the onset of the second subband.[20] To understand this disagreement, the intersubband scattering rate is neglected in a first step. The Lei-Ting mobility can be written (denoting by R_i the intrasubband scattering rate in subband i):

$$\mu_{\text{LT}}=(e/m)[(N_0/N)R_0+(N_1/N)R_1]^{-1} ,$$

whereas the Boltzmann mobility is derived by writing the total conductivity as the sum of the conductivity of each subband. This means that the subbands are handled as two independent conductors:

$$\mu_B=(e/m)[(N_0/N)(1/R_0)+(N_1/N)(1/R_1)] .$$

Since $(N_1/N)R_1$ is large [see Fig. 1(b)], R_1 is very large and the Boltzmann mobility should remain unchanged at the onset of the upper subband: the Boltzmann mobility drop should be of the order of N_1/N at the onset of the upper subband because the subband conductivities are additive, as for two independent conductors. Conversely, in the present approach the scattering rates are additive because the subbands are strongly coupled by the Coulomb interaction and the two-subband electron gas is handled as a whole. In that sense, the mobility drop calculated here may be attributed to the Coulomb scattering of the subband 0 carriers on the very low mobility carriers lying at the bottom of the upper subband.

When the impurity intersubband scattering is now included, the mobility drop derived from the coupled Boltzmann equations is likely to come from the balance on the subband population exchange rates, which couples the subband relaxation times to each other.[14] The interpretation of such a coupling could be as follows: because of the intersubband scattering, the carriers of the ground subband will spend some time in the upper subband where they experience an intense impurity scattering. However, the mobility is still derived by summing the subband conductivities: this means that the Coulomb coupling between the subbands due to $V^{1,1}_{0,0}$ is ignored whereas $V^{1,1}_{0,0}$ is as large as $V^{0,0}_{0,0}$ or $V^{1,1}_{1,1}$. When the Coulomb interaction between the subbands is fully taken into account, as in the Lei-Ting approach, coupling the subband relaxation times through the intersubband scattering rates is irrelevant since the balance on the subbands population exchange rates is necessarily fulfilled to first order in the electric field.

In the Boltzmann approach, the Coulomb interaction is only taken into account through screening, but here again another difference comes out. In our approach, the Coulomb interaction between the two subbands is fully embodied in the polarizability of the 2DEG, independently of the impurity potential. Terms involved in R_0 and R_1 (see Appendix B) are proportional either to $|G^0_0(\mathbf{z}_i,\mathbf{q})|^2$ or to $|G^1_1(\mathbf{z}_i,\mathbf{q})|^2$. In the Boltzmann approach,[14] on the contrary, screening is handled separately on its own and the intrasubband matrix elements of the impurity potential are mixed through the dielectric screening function. The ground subband scattering rate is derived from the impurity potential through

$$|V_{\text{imp}}/\epsilon_{00,00}|^2 \sim |[(1-V^{1,1}_{1,1}P^1_1)G^0_0 + (V^{1,1}_{0,0}P^1_1G^1_1)]/\epsilon|^2 .$$

In that case, the physical meaning of the crossed terms involving $G^0_0G^1_1$ is unclear. Moreover, it seems inconsistent to keep the intersubband Coulomb interaction $V^{1,1}_{0,0}$ in the screening terms and at the same time, to treat the two subbands as two decoupled conductors (i.e., summing up the conductivities to get the total conductivity).

The disagreement on the mobility discussed here is reminiscent of the difference between the Boltzmann adiabatic mobility formula where relaxation times are averaged and the isothermal mobility theory focuses on relaxation rates by fully taking into account the electric-field potential and the electron-electron Coulomb interaction.[21,15] From the above discussion it follows that the Coulomb interaction shows up not only in the screening of the scattering potentials but also in the way that the scattering rates are averaged: averaging the relaxation times as in the Boltzmann mobility means that the conductivities of the different carriers are added to each other, neglecting in part the Coulomb interaction between them. The mobility of a two-subband electronic system clearly enlightens the difference between the Lei and Ting balance equations for nonlinear electronic transport and a Boltzmann approach,[22] and the different behaviors predicted for the low-field mobility may provide an experimental way to resolve the controversy between them.

IV. HIGH-FIELD TRANSPORT

A. Experimental details

A detailed characterization of the sample used in our high-field transport experiments has been reported (sample 3 in Ref. 23). The parameters of this GaAs/$Ga_xAl_{1-x}As$ multiple-quantum-well sample are listed in Table I.

TABLE I. The parameters of the sample studied under high-field transport conditions. The structural parameters are deduced from x-ray measurements; the electronic density and the low-field low-temperature mobility are deduced from Hall and Shubnikov–de Haas measurements.

Well thickness L (Å)	Barrier thickness L_b (Å)	Doped $Ga_xAl_{1-x}As$ L_d (Å)	Spacer (Å)	x_{Al}	N_D (10^{17} cm^{-3})	N (10^{11} cm^{-2})	Mobility (4.2 K) (m^2/V s)
274	1089	121	484	0.24	2.75	3.51	33

To minimize the Joule heating, 1-μs electric field pulses, with a duty cycle lower than 10^{-2}, were applied along the heterolayers. The photoluminescence was excited with an argon laser and the optical power was kept below 100 mW/cm^2 to prevent optical heating. By using simple gating techniques, the photoluminescence from the samples was collected only during the electric pulses. Assuming that the low density (10^8 cm^{-2}) of optically excited holes thermalizes with the high-density electron gas, the luminescence intensity decreases as

$$I_{\mathrm{PL}} \sim \exp(-\hbar\omega/kT_e) ,$$

where T_e is the electronic temperature, provided that the emitted photon energy $\hbar\omega$ is well above the sum of the band gap and of the Fermi energy and that the density of states is staircase shaped. It should be noticed that for such wide quantum wells, a large number of hole quantum levels are involved in the valence band at finite temperature. Consequently, the hole density of state is rather a three-dimensional one, behaving as the square root of the energy. Therefore, the hot-carrier temperature may be experimentally slightly overestimated. Performing high-field Hall measurements, we checked that the electron density remained constant within experimental accuracy (20%).

B. Theoretical results

The numerical values used for the material constants in our simulations are listed in Table II. We plot in Fig. 2 the Fermi levels, together with the renormalized quantum levels versus the carrier temperature. At low electric fields, the Fermi levels are equal, in agreement with the preceding paragraph where their splitting has been demonstrated to increase at least quadratically with the electric field. Then, the upper-subband Fermi level rises above the lower-subband Fermi level before they cross around 80 K. A careful inspection of the origin of the intersubband transitions shows that LO phonons mainly transfer electrons from the upper subband to the ground subband, while scattering on impurities transfers carriers from the ground subband to the upper subband. At low temperatures, the impurity associated behavior dominates, raising the upper-subband Fermi level above the ground-subband Fermi level, whereas at high temperatures the LO phonons overcome. The splitting of the Fermi levels, which accounts for the balance on the exchange of particles between the two subbands, is the counterpart of the splitting between the lattice temperature T and the hot-electron temperature T_e: as is obvious from (2), the energy absorbed and turned into heat through scattering on the randomly distributed impurities, is transferred to the lattice through phonon emission. Therefore, the increase of the relative electron-gas temperature is due in a first step to the scattering of impurities (Fig. 3). This rise of temperature is lessened because of the transfer of carriers by impurity intersubband scattering, which raises the upper-subband Fermi level above the ground-subband Fermi level: for the same average energy the temperature is lower than what it would be if the Fermi levels were equal. After a slowing down in the growth speed of the temperature due also to the increasing efficiency of the LO-phonon emission because of the nonlinear Bose factor $B[(\hbar\omega_{\mathrm{LO}}-\hbar\mathbf{v}_d\cdot\mathbf{q})/kT_e]$, the temperature T_e increases again more steeply. For drift velocities above 1.5×10^7 cm/s, the range of wave vectors, where $\omega_{\mathrm{LO}}-\mathbf{v}_d\cdot\mathbf{q}$ is negative becomes noticeable ($q \geq 3\times10^6$ cm^{-1}) and increases with the drift velocity. In that case, the relative electron gas absorbs some kinetic energy from the center-of-mass motion mainly through LO-phonon–electron interaction and turns it into heat by Coulomb interactions within the electron gas.

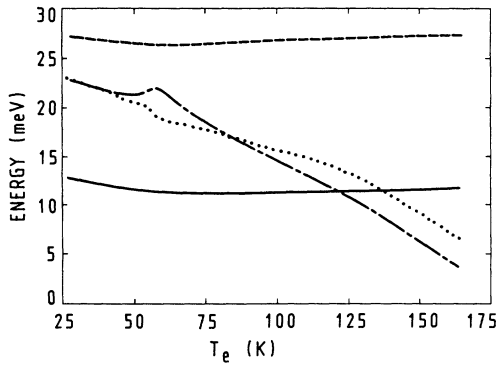

FIG. 2. Energies at the bottom of the subbands and Fermi levels against the carrier temperature: ground-subband energy (full curve) and Fermi level (dotted curve); upper subband energy (dashed curve) and Fermi level (dashed-dotted curve). The energies are measured with reference to the bulk GaAs conduction band. The phonon lifetime is $\tau_{\mathrm{ph}}=0$ ps.

C. Discussion

To characterize the electron-energy-loss rate, the reciprocal electron temperature is plotted against the electric-field power input per electron for three LO-phonon lifetimes (Fig. 4). It should be mentioned that the electron temperature measures the internal energy of the relative electron gas, whereas the electric-field power is applied to the drifting 2DEG, the energy of which is

TABLE II. The numerical values of the GaAs/$Ga_xAl_{1-x}As$ material constants used in the numerical simulations.

κ	κ_∞	v_{st} (cm/s)	v_{sl} (cm/s)	ρ (g/cm^3)	D (eV)	h_{14} (V/cm)	$\hbar\omega_{\mathrm{LO}}$ (meV)
12.90	10.92	3×10^5	5.3×10^5	5.3	12	1.2×10^7	36

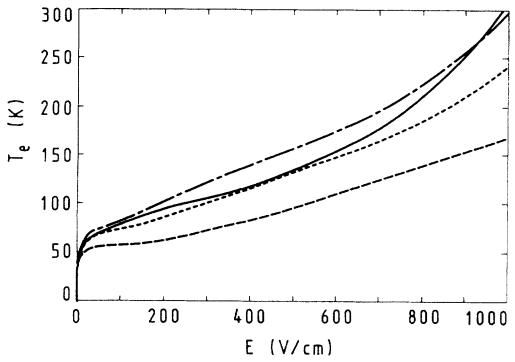

FIG. 3. Hot-carrier temperature vs electric field: experimental data (full curve); theoretical curves without hot phonons (dashed curve), with hot phonons for a phonon lifetime $\tau_{ph}=3$ ps (dotted curve) and $\tau_{ph}=7$ ps (dashed-dotted curve).

the sum of the kinetic energy of the center-of-mass and of the thermal energy of the relative electron gas. The better agreement with experiment is found for a phonon lifetime between 3 and 7 ps.

The nonequilibrium phonon population is highly anisotropic with a peaked distribution in the direction of the drift velocity (Fig. 5). This anisotropy comes from the Doppler shift of the LO-phonon frequency ($\omega_{LO}\rightarrow\omega_{LO}-\mathbf{v}_d\cdot\mathbf{q}$), which enhances the electron–LO-phonon coupling for LO modes having a phase velocity along the 2DEG drift velocity. Therefore a LO-phonon gas drifts with the electron gas and exchanges momentum with it. The peak values of the nonequilibrium LO-phonon population are associated with wave vectors q, such that $\omega_{LO}-\mathbf{v}_d\cdot\mathbf{q}\approx 0$. This means that the relative electron gas interacts mainly with those LO phonons that have a phase velocity nearly equal to the drift velocity.

The experimental drift velocity is plotted in Fig. 6. The agreement with theory is fairly good: the calculated velocity is only about 15% higher than the experimental one at the highest electric field. Such a disagreement may be due to an additional scattering on a few low-energy electrons in the third subband or to an overestimation of 2DEG density at high electric fields and a correlative underestimation of the drift velocity, since the high-field

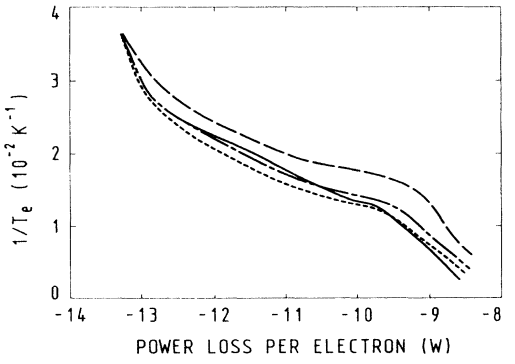

FIG. 4. Inverse electron temperature vs power loss per electron. The full line accounts for the experimental results. Theoretical results are reported for three LO-phonon lifetimes: $\tau_{ph}=0$ ps (dashed curve), $\tau_{ph}=3$ ps (dashed-dotted curve), and $\tau_{ph}=7$ ps (dotted curve).

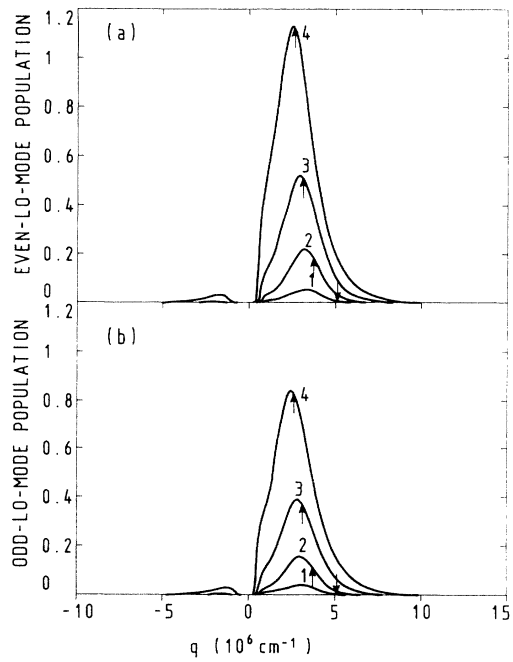

FIG. 5. Hot-LO-phonon population vs phonon wave vector in the electric field direction: (a) first even LO mode; (b) first odd LO mode. The phonon lifetime is $\tau_{ph}=3$ ps and the arrows point on the wave vector such that $\omega_{LO}-\mathbf{v}_d\cdot\mathbf{q}=0$. The drift velocities and the carrier temperatures are (1) $v_d=1.08\times10^7$ cm/s, $T_e=71$ K; (2) $v_d=1.48\times10^7$ cm/s, $T_e=86$ K; (3) $v_d=1.76\times10^7$ cm/s, $T_e=135$ K; (4) $v_d=2.1\times10^7$ cm/s, $T_e=241$ K.

Hall measurements accuracy is only 20%. The drift velocity is only weakly reduced by a finite LO-phonon lifetime, since the overall momentum is not relaxed within the phonon branch and is reabsorbed together with the LO-phonon energy.

The question of the momentum relaxation rate of drifting hot LO phonons arises at first because of the anisotro-

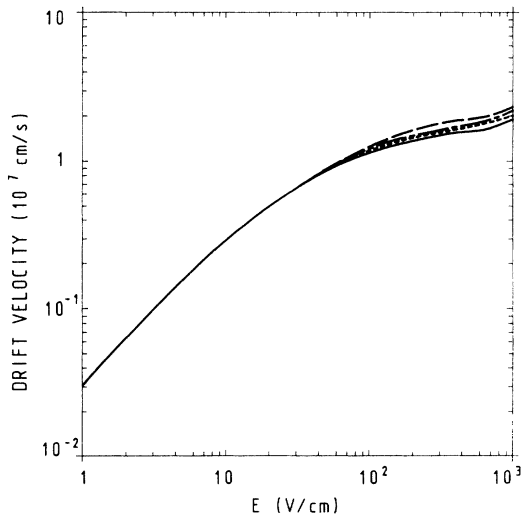

FIG. 6. Drift velocities vs electric field. The full line accounts for the experimental results. Theoretical results are reported for three LO-phonon lifetimes: $\tau_{ph}=0$ ps (dashed curve), $\tau_{ph}=3$ ps (dashed-dotted curve), and $\tau_{ph}=7$ ps (dotted curve).

py of the electron–LO-phonon interaction, which is enhanced for LO modes having their wave vectors in the direction of the drift velocity. If the nonequilibrium LO-phonon momentum were completely relaxed within the LO-phonon modes by intrabranch scattering events, keeping the same phonon population lifetime would greatly inhibit the reduction of the electron-energy-loss rate due to hot phonons because the isotropic nonequilibrium phonon population would be quite small, whereas the electron–LO-phonon coupling would remain highly anisotropic. On the other hand, keeping the same reduction in the electron-energy-loss rate with nondrifting hot phonons would require a high nonequilibrium phonon population for these wave vectors, where the electron-phonon coupling is strong (see Fig. 5). Since the hot-phonon population level is equal in any direction for nondrifting phonons, unlikely large phonon lifetimes would be required. In all the above, nondrifting hot phonons have been discussed assuming a given drift velocity and an electron-phonon coupling that is reduced to wave vectors lying along the drift velocity. If we now take into account that the electron–LO-phonon coupling is not strictly zero for modes that do not move along the drift velocity, a nonequilibrium phonon population in all directions is still required in order to keep the electron-energy-loss rate small even if the phonon lifetime is not as large as in the total anisotropic coupling case. Momentum reabsorption from this random phonon distribution will imply a reduction of the drift velocity, which would be in disagreement with the experimental results. Therefore, in all respects hot LO phonons are likely to drift together with the electron gas.

It is worth noting that we recover a quasiequilibrium state on the subband populations in the presence of hot phonons. At low fields, the relative impurity contribution to the Fermi level's splitting is reduced because the electron gas is hotter, and at high fields the LO-phonon reabsorption by intersubband scattering transfers electrons back from the ground to the upper subband.

The momentum relaxation rates per the center-of-mass momentum $Nm\mathbf{v}_d$ are plotted in Fig. 7 for scattering on impurities and phonons, together with their sum, which is equal to $\mathbf{r}_E = e\mathbf{E}/(mv_d)$ and with the scattering rate deduced from the low-field experimental mobility $\mu, r_\mu = e/(m\mu)$. The high-field scattering rate first increases more steeply than the scattering rate derived from the low-field mobility. This behavior, which is well pronounced in the absence of hot phonons, cannot be associated with a large nonequilibrium phonon population but with the electron–LO-phonon interaction enhancement by the Doppler shift of the LO-phonon frequency for a nonvanishing drift velocity: the emission threshold for LO phonons is reduced from $\hbar\omega_{\mathrm{LO}}$ to $\hbar\omega_{\mathrm{LO}} - \hbar\mathbf{v}_d \cdot \mathbf{q}$ and therefore the temperature required for LO-phonon emission when the 2DEG is drifting is lower than in the case of low-field mobility experiments. As the lattice temperature is raised in low-field experiments, the equilibrium LO-phonon population becomes noticeable and its absorption by the 2DEG is no longer negligible against its emission: the low-field scattering rate overtakes the high-field scattering rate. The energy relaxation

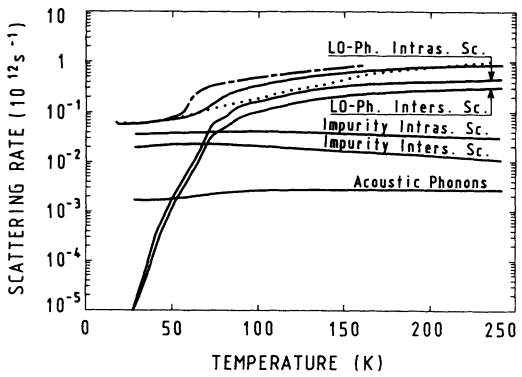

FIG. 7. Momentum relaxation rates per the center-of-mass momentum Nmv_d vs hot-carrier temperature for intrasubband scattering on acoustic phonons, LO phonons, impurities, and for intersubband scattering on LO phonons and impurities (the LO-phonon lifetime is $\tau_{\mathrm{ph}} = 3$ ps). Scattering rate derived from the high-field mobility $r_E = eE/(mv_d)$ vs carrier temperature: $\tau_{\mathrm{ph}} = 3$ ps (full curve); $\tau_{\mathrm{ph}} = 0$ ps (dashed-dotted curve). Scattering rate derived from the experimental low-field mobility $\mu, r_\mu = e/(m\mu)$ vs lattice temperature (solid circles).

rates per the LO-phonon energy $\hbar\omega_{\mathrm{LO}}$ and per electron are also plotted for two LO-phonon lifteimes (Fig. 8). The mean time for the emission of $\hbar\omega_{\mathrm{LO}}$ per electron stays beyond 1 ps.

In order to examine the influence of the drift velocity on the energy-loss rate, we have considered the samples reported in Ref. 1. The carrier density and the well width of sample 2 are quite similar to our sample ones, and we will now compare these two samples. The only difference arises from the low-field mobility, which is $\mu = 79\,000$ cm^2/V s against $\mu = 330\,000$ cm^2/V s for our sample. For a given hot-electron-gas temperature, the low-mobility sample power-loss rate is almost one order of magnitude smaller than the high-mobility one (Fig. 9). The energy supplied to the 2DEG by the electric field is in part turned into heat through dissipative mechanisms such as scattering on randomly distributed impurities. This part is well characterized by the hot-carrier temperature and is transferred to the phonon bath through the emission of $\hbar\omega_{\mathrm{LO}} - \hbar\mathbf{v}_d \cdot \mathbf{q}$. The other part is transferred directly to the phonon bath through the center-of-mass motion by emission of the Doppler energy $\hbar\mathbf{v}_d \cdot \mathbf{q}$. In oth-

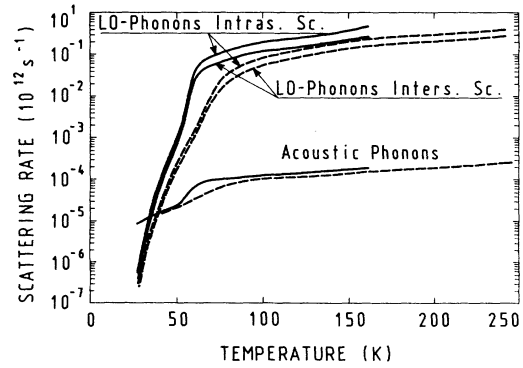

FIG. 8. Energy relaxation rates per $\hbar\omega_{\mathrm{LO}}$ and per electron vs hot-carrier temperature for two LO-phonon lifetimes: $\tau_{\mathrm{ph}} = 0$ ps (full curves), and $\tau_{\mathrm{ph}} = 3$ (dashed curves).

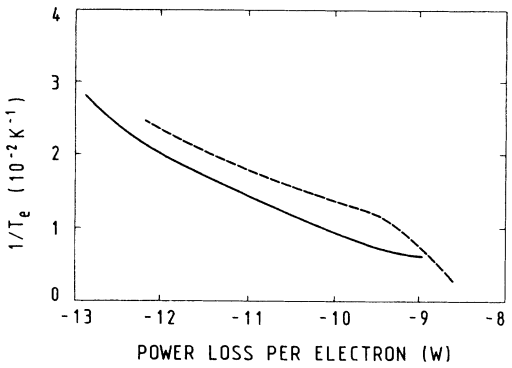

FIG. 9. Inverse electron temperature vs power loss per electron. Experimental results are reported for two samples: full curve (sample 2, Ref. 1, $\mu=7.9$ m^2/V s), dashed curve (sample 3, Ref. 17, $\mu=33$ m^2/V s).

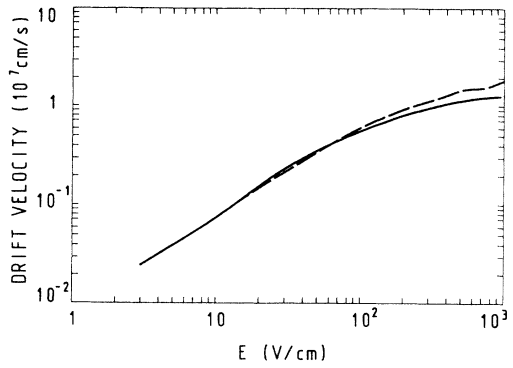

FIG. 11. Drift velocities vs electric field for sample 2 of Ref. 1. The full line accounts for the experimental results. Theoretical results are reported for a LO-phonon lifetime $\tau_{ph}=7$ ps (dashed curve).

er words, the relative electron-gas temperature does not fully characterize the whole energy supplied by the electric field to the drifting 2DEG, the state of which is determined by both the drift velocity and the electron temperature. In spite of the large difference between the experimental power-loss diagrams, the LO-phonon lifetime, which is necessary to account for the energy-loss rates, is about 5 ps whatever the sample investigated (Fig. 10). Once again, the agreement between the calculated drift velocities and the experiments is fairly good (Fig. 11), assuming that the nonequilibrium hot LO phonons are drifting.

V. CONCLUSION

The electron–LO-phonon coupling in GaAs/$Ga_xAl_{1-x}As$ modulation doped quantum wells has been investigated through steady-state transport experiments performed on a wide quantum well by measuring both the drift velocity and the hot-carrier temperature. Within a two-subband model, the influence of intersubband scattering has been taken into account for the relaxation of the 2DEG energy and momentum and for the carrier density distribution between the two subbands. The investigations reported here are based on the balance description of the high-field transport of Lei and Ting, which separates the center-of-mass variables from the relative variables of the electrons. It is thus possible to separate the thermal motion of the electron system from its drift motion and to analyze the influence of the electric-field power input on each of them. Therefore, the temperature against power-loss diagrams are not fully representative of the electron–LO-phonon coupling. For a given temperature, the higher the low-field mobility, the higher the electric-field power input. When the decay of LO phonons into acoustic modes is described by a unique lifetime, the agreement with the experiments requires a mean time of about 5 ps. For such a lifetime and according to the drift velocity calculations, the nonequilibrium LO-phonon dephasing time should be of the same order of magnitude as the population relaxation time. As a consequence, the nonequilibrium hot phonons drift with a phase velocity roughly equal to the electron drift velocity. The splitting between the subbands Fermi levels arises from the competition between the impurity intersubband scattering, which transfers carriers in the upper subband, and the intersubband LO-phonon emission, which brings carriers back into the ground subband. The overall result is rather weak and does not affect the 2DEG temperature to a large extent. Finally, it has been shown that the low-field mobility is mainly reduced at the onset of the second subband by intrasubband scattering. It has been argued that the high-mobility electrons lying at the Fermi level of the ground subband are efficiently scattered by the low-mobility carriers of the upper subband through the electron-electron Coulomb interaction.

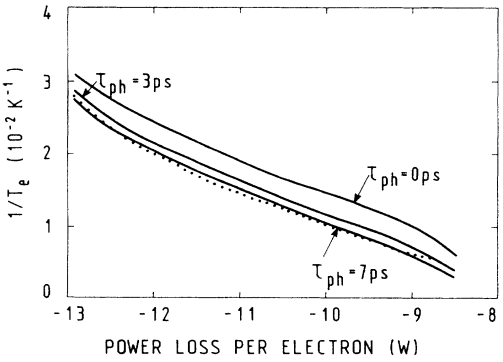

FIG. 10. Inverse electron temperature vs power loss per electron (sample 2, Ref. 1). The full lines account for the theoretical results for three LO-phonon lifetimes. Experimental results are also reported (solid circles).

APPENDIX A

To derive the balance equation for the momentum exchanges, the statistical expectation of the rate of change of the total impulsion, $\dot{\mathbf{P}}=(1/i\hbar)[\mathbf{P},H]$ is calculated:

$$Ne\mathbf{E}=\sum_{\mathbf{q}}\hbar\mathbf{q}\left\{\sum_{i,\sigma,\sigma'}[G_{\sigma}^{\sigma'}(\mathbf{z}_i,\mathbf{q})e^2/(2A\epsilon_0\kappa q)]^2(1/\hbar)[-\mathrm{Im}\Pi_{\sigma}^{\sigma'}(\mathbf{q},\mathbf{v}_d\cdot\mathbf{q})]\right.$$
$$+\sum_{\lambda,q_z,\sigma}\Gamma_{\sigma}(\lambda_{\mathrm{ac}},\mathbf{Q},\omega_{\lambda,\mathbf{Q}}-\mathbf{v}_d\cdot\mathbf{q})\{B[(\hbar\omega_{\lambda,\mathbf{Q}}-\hbar\mathbf{v}_d\cdot\mathbf{q})/kT_e]-B(\hbar\omega_{\lambda,\mathbf{Q}}/kT)\}$$
$$\left.+\sum_{\lambda,\sigma,\sigma'}\Gamma_{\sigma}^{\sigma'}(\lambda,\mathbf{q},\omega_{\mathrm{LO}}-\mathbf{v}_d\cdot\mathbf{q})\{B[(\hbar\omega_{\mathrm{LO}}-\hbar\mathbf{v}_d\cdot\mathbf{q}+\mu_{\sigma'}-\mu_{\sigma})/kT_e]-B(\hbar\omega_{\mathrm{LO}}/kT_{\lambda,\mathbf{q}})\}\right\} \tag{A1}$$

with

$$\Gamma_{\sigma}^{\sigma}(\lambda_{\mathrm{ac}},\mathbf{q},\omega)=-(2/\hbar)|M_{\mathrm{ac}}(\mathbf{Q},\lambda)I_{\sigma}^{\sigma}(q_z)|^2\mathrm{Im}\Pi_{\sigma}^{\sigma}(\mathbf{q},\omega)\ ,$$
$$\Gamma_{\sigma}^{\sigma'}(\lambda,\mathbf{q},\omega)=-(2/\hbar)|M_{\mathrm{opt}}(\mathbf{q},\lambda)I_{\sigma}^{\sigma'}(q_z)|^2\mathrm{Im}\pi_{\sigma}^{\sigma'}(\mathbf{q},\omega)\ .$$

We now consider, the rate of change of the relative electron-gas energy $\dot{H}_e=(1/i\hbar)[H_e,H]$. This rate originates solely from the relative electron kinetic energy. We get an equation between the energy absorption due to impurities and the energy emission through the electron-phonon interactions:

$$\sum_{\mathbf{q}}\hbar\mathbf{v}_d\cdot\mathbf{q}\sum_{i,\sigma,\sigma'}[G_{\sigma}^{\sigma'}(\mathbf{z}_i,\mathbf{q})e^2/(2A\epsilon_0\kappa q)]^2(1/\hbar)[-\mathrm{Im}\Pi_{\sigma}^{\sigma'}(\mathbf{q},\mathbf{v}_d\cdot\mathbf{q})]$$
$$=\sum_{q}\left\{\sum_{\lambda,q_z,\sigma}(\hbar\omega_{\lambda,\mathbf{Q}}-\hbar\mathbf{v}_d\cdot\mathbf{q})\Gamma_{\sigma}(\lambda_{\mathrm{ac}},\mathbf{Q},\omega_{\lambda,\mathbf{Q}}-\mathbf{v}_d\cdot\mathbf{q})\{B[(\hbar\omega_{\lambda,\mathbf{Q}}-\hbar\mathbf{v}_d\cdot\mathbf{q})/kT_e]-B(\hbar\omega_{\lambda,\mathbf{Q}}/kT)\}\right.$$
$$\left.+\sum_{\lambda,\sigma,\sigma'}(\hbar\omega_{\mathrm{LO}}-\hbar\mathbf{v}_d\cdot\mathbf{q})\Gamma_{\sigma}^{\sigma'}(\lambda,\mathbf{q},\omega_{\mathrm{LO}}-\mathbf{v}_d\cdot\mathbf{q})\{B[(\hbar\omega_{\mathrm{LO}}-\hbar\mathbf{v}_d\cdot\mathbf{q}+\mu_{\sigma'}-\mu_{\sigma})/kT_e]-B(\hbar\omega_{\mathrm{LO}}/kT_{\lambda,\mathbf{q}})\}\right\}\ . \tag{A2}$$

Combining Eqs. (A1) and Eq. (A2), we get the equation between the electric-field power supplied to the 2DEG and the rate of energy loss through the emission of phonons:

$$Ne\mathbf{E}\cdot\mathbf{v}_d=\sum_{\mathbf{q}}\left\{\sum_{\lambda,q_z,\sigma}\hbar\omega_{\lambda,\mathbf{Q}}\Gamma_{\sigma}(\lambda_{\mathrm{ac}},\mathbf{Q},\omega_{\lambda,\mathbf{Q}}-\mathbf{v}_d\cdot\mathbf{q})\right\}\{B[\hbar\omega_{\lambda,\mathbf{Q}}-\hbar\mathbf{v}_d\cdot\mathbf{q})/kT_e]-B(\hbar\omega_{\lambda,\mathbf{Q}}/kT)\}$$
$$+\sum_{\lambda,\sigma,\sigma'}\hbar\omega_{\mathrm{LO}}\Gamma_{\sigma}^{\sigma'}(\lambda,\mathbf{q},\omega_{\mathrm{LO}}-\mathbf{v}_d\cdot\mathbf{q})\{B[(\hbar\omega_{\mathrm{LO}}-\hbar\mathbf{v}_d\cdot\mathbf{q}+\mu_{\sigma'}-\mu_{\sigma})/kT_e]-B(\hbar\omega_{\mathrm{LO}}/kT_{\lambda,\mathbf{q}})\}\ .$$

Ignoring all the exchanges of particles between the subbands through electron-electron scattering, the vanishing rate of change of the electron population of the subband σ is expressed as

$$\sum_{\mathbf{q}}\sum_{i}[G_{\sigma}^{\sigma'}(\mathbf{z}_i,\mathbf{q})e^2/(2A\epsilon_0\kappa q)]^2(1/\hbar)[\mathrm{Im}\Pi_{\sigma}^{\sigma'}(\mathbf{q},\mathbf{v}_d\cdot\mathbf{q})-\mathrm{Im}\Pi_{\sigma'}^{\sigma}(\mathbf{q},\mathbf{v}_d\cdot\mathbf{q})]$$
$$=\sum_{q}\sum_{\lambda}(\Gamma_{\sigma'}^{\sigma}(\lambda,\mathbf{q},\omega_{\mathrm{LO}}-\mathbf{v}_d\cdot\mathbf{q})\{B[(\hbar\omega_{\mathrm{LO}}-\hbar\mathbf{v}_d\cdot\mathbf{q}+\mu_{\sigma}-\mu_{\sigma'})/kT_e]-B(\hbar\omega_{\mathrm{LO}}/kT_{\lambda,\mathbf{q}})\}$$
$$-\Gamma_{\sigma}^{\sigma'}(\lambda,\mathbf{q},\omega_{\mathrm{LO}}-\mathbf{v}_d\cdot\mathbf{q})\{B[(\hbar\omega_{\mathrm{LO}}-\hbar\mathbf{v}_d\cdot\mathbf{q}+\mu_{\sigma'}-\mu_{\sigma})/kT_e]-B(\hbar\omega_{\mathrm{LO}}/kT_{\lambda,\mathbf{q}})\})\ . \tag{A3}$$

The decay of LO-phonon modes populations through anharmonic processes is heuristically described with a unique lifetime τ_{ph}:

$$\langle N_{\lambda,\mathbf{q}}\rangle_{\mathrm{ph\text{-}ph}}=-(\langle N_{\lambda,\mathbf{q}}\rangle-N_{\mathrm{eq}})/\tau_{\mathrm{ph}}\ \text{ with }\ N_{\mathrm{eq}}=1/[\exp(\hbar\omega_{\mathrm{LO}}/kT)-1]\ .$$

Finally, we have

$$\langle N_{\lambda,\mathbf{q}}\rangle=B[(\hbar\omega_{\mathrm{LO}}-\hbar\mathbf{v}_d\cdot\mathbf{q}+\mu_{\alpha'}-\mu_{\alpha})/kT_e]+\frac{N_{\mathrm{eq}}-B[(\hbar\omega_{\mathrm{LO}}-\hbar\mathbf{v}_d\cdot\mathbf{q}+\mu_{\alpha'}-\mu_{\alpha})/kT_e]}{1+\tau_{\mathrm{ph}}\sum_{\sigma,\sigma'}\Gamma_{\sigma}^{\sigma'}(\lambda,\mathbf{q},\omega_{\mathrm{LO}}-\mathbf{v}_d\cdot\mathbf{q})}$$
$$+\left\{\frac{\tau_{\mathrm{ph}}\Gamma_{\alpha'}^{\alpha}(\lambda,\mathbf{q},\omega_{\mathrm{LO}}-\mathbf{v}_d\cdot\mathbf{q})}{1+\tau_{\mathrm{ph}}\sum_{\sigma,\sigma'}\Gamma_{\sigma}^{\sigma'}(\lambda,\mathbf{q},\omega_{\mathrm{LO}}-\mathbf{v}_d\cdot\mathbf{q})}\right.$$
$$\left.\times\{B[(\hbar\omega_{\mathrm{LO}}-\hbar\mathbf{v}_d\cdot\mathbf{q}+\mu_{\alpha}-\mu_{\alpha'})/kT_e]-B[(\hbar\omega_{\mathrm{LO}}-\hbar\mathbf{v}_d\cdot\mathbf{q}+\mu_{\alpha'}-\mu_{\alpha})/kT_e]\}\right\}\ , \tag{A4}$$

with $\alpha'=\alpha$ for even LO modes and $\alpha'\neq\alpha$ for odd LO modes.

APPENDIX B

We give below the full expression of the intrasubband and intersubband scattering rates for the case of low-temperature impurity scattering:

$$R_{\text{intra}}=(N_0/N)R_0+(N_1/N)R_1 ,$$

$$R_0=(X/N_0)\sum_i \int_0^{2k_{f_0}} \frac{dq}{|\epsilon|^2(4k_{f_0^2}-q^2)^{1/2}} \times\{|G_0^0(z_i,q)|^2[1-(V_{1,1}^{1,1}-V_{0,0}^{1,1})P_1^1(q,0)][1-V_{1,1}^{1,1}P_1^1(q,0)] -|G_1^1(z_i,q)|^2[1-(V_{1,1}^{1,1}-V_{0,0}^{1,1})P_1^1(q,0)][-V_{0,0}^{1,1}P_1^1(q,0)]\} ,$$

$$R_{1=}(X/N_1)\sum_i \int_0^{2k_{f_1}} \frac{dq}{|\epsilon|^2(4k_{f_1^2}-q^2)^{1/2}} \times\{|G_1^1(z_i,q)|^2[1-(V_{0,0}^{0,0}-V_{0,0}^{1,1})P_0^0(q,0)][1-V_{0,0}^{0,0}P_0^0(q,0)] -|G_0^0(z_i,q)|^2[1-(V_{0,0}^{0,0}-V_{1,1}^{0,0})P_0^0(q,0)][-V_{1,1}^{0,0}P_0^0(q,0)]\}$$

$$R_{\text{inter}}=(X/N)\left[\sum_i \int_{k_{f_0}-k_{f_1}}^{k_{f_0}+k_{f_1}} dq \frac{(1+\Delta_0^1/q^2)|G_0^1(z_i,q)|^2}{[4k_{f_0^2}-q^2(1+\Delta_0^1/q^2)^2]^{1/2}} + \int_{k_{f_0}-k_{f_1}}^{k_{f_0}+k_{f_1}} dq \frac{(1-\Delta_0^1/q^2)|G_0^1(z_i,q)|^2}{[4k_{f_1^2}-q^2(1-\Delta_0^1 q^2)^2]^{1/2}}\right] ,$$

$$k_{f_0}=[2m(\mu-E_0)/\hbar^2]^{1/2},\quad k_{f_1}=[2m(\mu-E_1)/\hbar^2]^{1/2},\quad \Delta_0^1=2m(E_1-E_0)/\hbar^2 ,$$

$$\epsilon=[1-V_{0,0}^{0,0}P_0^0(q,0)][1-V_{1,1}^{1,1}P_1^1(q,0)]-V_{1,1}^{0,0}P_0^0(q,0)V_{0,0}^{1,1}P_1^1(q,0) ,$$

$$X=(2m/\hbar^3)[e^2/(4\pi\epsilon_0\kappa)]^2 .$$

Since subbands are fully relevant to characterize free particles in a quantum well, the terms due to the intrasubband scatterings can be clearly identified, as they involve free-particle absorption in each subband. For instance, in the ground-subband case, these terms are proportional to $d\,\text{Im}P_0^0(q,\omega)/d\omega$ through the factor $1/(4kf_0^2-q^2)^{1/2}$ for the ground subband.

[1] J. Shah, A. Pinczuk, A. C. Gossard, and W. Wiegmann, Phys. Rev. Lett. **54**, 2045 (1985); J. Shah, A. Pinczuk, H. L. Störmer, A. C. Gossard, and W. Wiegmann, Appl. Phys. Lett. **44**, 322 (1984).

[2] X. L. Lei and N. J. M. Horing, Phys. Rev. B **35**, 6281 (1987).

[3] C. H. Yang, J. M. Carlson-Swindle, S. A. Lyon, and J. M. Worlock, Phys. Rev. Lett. **55**, 2359 (1985).

[4] B. K. Ridley, Semicond. Sci. Technol. **4**, 1142 (1989); B. K. Ridley, Rep. Prog. Phys. **54**, 169 (1991).

[5] S. Das Sarma, J. Jain, and R. Jalabert, Phys. Rev. B **41**, 3561 (1990).

[6] P. Lugli and S. M. Goodnick, Phys. Rev. Lett. **59**, 716 (1987).

[7] N. Balkan, B. K. Ridley, M. Emeny, and I. Goodridge, Semicond. Sci. Technol. **4**, 852 (1989).

[8] C. Guillemot, F. Clérot, P. Auvray, M. Baudet, M. Gauneau, and A. Regreny, Superlatt. Microstruct. **8**, 259 (1990).

[9] D. V. D. Linde, J. Kuhl, and H. Klingenberg, Phys. Rev. Lett. **44**, 1505 (1980).

[10] F. Vallée and F. Bogani, Phys. Rev. B **43**, 12 049 (1991).

[11] K. T. Tsen, R. P. Joshi, D. K. Ferry, and H. Morkoç, Phys. Rev. B **39**, 6025 (1989).

[12] R. Gupta and B. K. Ridley, Solid State Electron. **32**, 1241 (1989).

[13] X. L. Lei and C. S. Ting, Phys. Rev. B **32**, 1112 (1985); X. L. Lei, D. Y. Xing, M. Liu, C. S. Ting, and J. L. Birman, *ibid.* **36**, 9134 (1987).

[14] S. Mori and T. Ando, J. Phys. Soc. Jpn. **48**, 865 (1980).

[15] X. L. Lei, Phys. Lett. A **148**, 384 (1990); Phys. Rev. B **41**, 8085 (1990).

[16] C. Guillemot and F. Clérot, Phys. Rev. B **44**, 6249 (1991). The bulk phonon coupling constants reported in Figs. 5 and 7 of this reference should be multiplied by a factor of 2. Therefore, the bulk-phonon and the quantized-phonon scattering rates are found to be equal for large quantum-well widths.

[17] R. Zimmermann, *Many-Particule Theory of Highly Excited Semiconductors,* Teubner—Texte zur Physik (Teubner, Leipzig, 1987), Vol. 18.

[18] C. Guillemot and F. Clérot (unpublished).

[19] G. Bongiovanni, J. L. Staehli, A. Bosacchi, and S. Franchi, Superlatt. Microstruct. **9**, 479 (1991).

[20] Intersubband scattering is reported in Ref. 14 for a larger subband spacing than here. Therefore, the wave vectors entering the scattering rates are larger than in our example, so that the weakness of the intersubband scattering as compared to the intrasubband scattering reported here is also meaningful for the case of Ref. 14.

[21] R. S. Fishman and G. D. Mahan, Phys. Rev. B **39**, 2990 (1989); R. S. Fishman, *ibid.* **39**, 2994 (1989); P. N. Argyres, *ibid.* **39**, 2982 (1989). See also Ref. 15.

[22] M. C. Marchetti and W. Cai, Phys. Rev. B **36**, 8159 (1987); X. L. Lei and C. S. Ting, *ibid.* **36**, 8162 (1987).

[23] C. Guillemot, M. Baudet, M. Gauneau, A. Regreny, and J. C. Portal, Phys. Rev. B **35**, 2799 (1987).